

Supporting information

Nickel binding with magnetite nanoparticles

Laura Fablet^{1,2}, Mathieu Pédrot¹, Fadi Choueikani², Isabelle Kieffer³, Olivier Proux³,
Anne-Catherine Pierson-Wickmann¹, Vyria Cagniard¹, Takumi Yomogida^{4,5}, Rémi
Marsac⁴

¹ Univ Rennes, CNRS, Géosciences Rennes – UMR 6118, F-35000 Rennes, France

² Synchrotron SOLEIL, l'Orme des Merisiers, Départementale 128, 91190 Saint-Aubin,
France

³ Univ. Grenoble Alpes, CNRS, IRD, INRAE, Météo France, OSUG, 38000 Grenoble, France

⁴ Université Paris Cité, Institut de physique du globe de Paris, CNRS, F-75005 Paris, France

⁵ Nuclear Safety Research Center, Japan Atomic Energy Agency, 2-4 Shirakata, Naka, Tokai,
Ibaraki, 319-1195, Japan

The supporting information section contains 12 pages, 8 reference, 7 figures and 3 tables.

Table S1 Corresponding total ($[\text{Ni}]_{\text{tot}}$), aqueous ($[\text{Ni}]_{\text{aq}}$) and solid ($[\text{Ni}]_{\text{s}}$) concentrations of Ni for R0.1 and R0.5.

$[\text{Ni}]_{\text{tot}}$ (mM)	$[\text{Ni}]_{\text{aq}}$ (mM)		$[\text{Ni}]_{\text{s}}$ (mM)	
	R0.1	R0.5	R0.1	R0.5
0.04	0.007	0	0.033	0.040
0.08	0.027	0.001	0.053	0.080
0.16	0.092	0.001	0.068	0.159
0.20	0.133	0.008	0.067	0.192
0.32	0.242	0.059	0.078	0.261
0.40	-	0.093	-	0.307
0.80	0.338	0.286	0.462	0.514
0.96	0.471	0.521	0.489	0.439
1.50	0.656	0.716	0.845	0.785
2.20	1.164	1.074	1.036	1.126
3.00	1.121	1.303	1.877	1.698

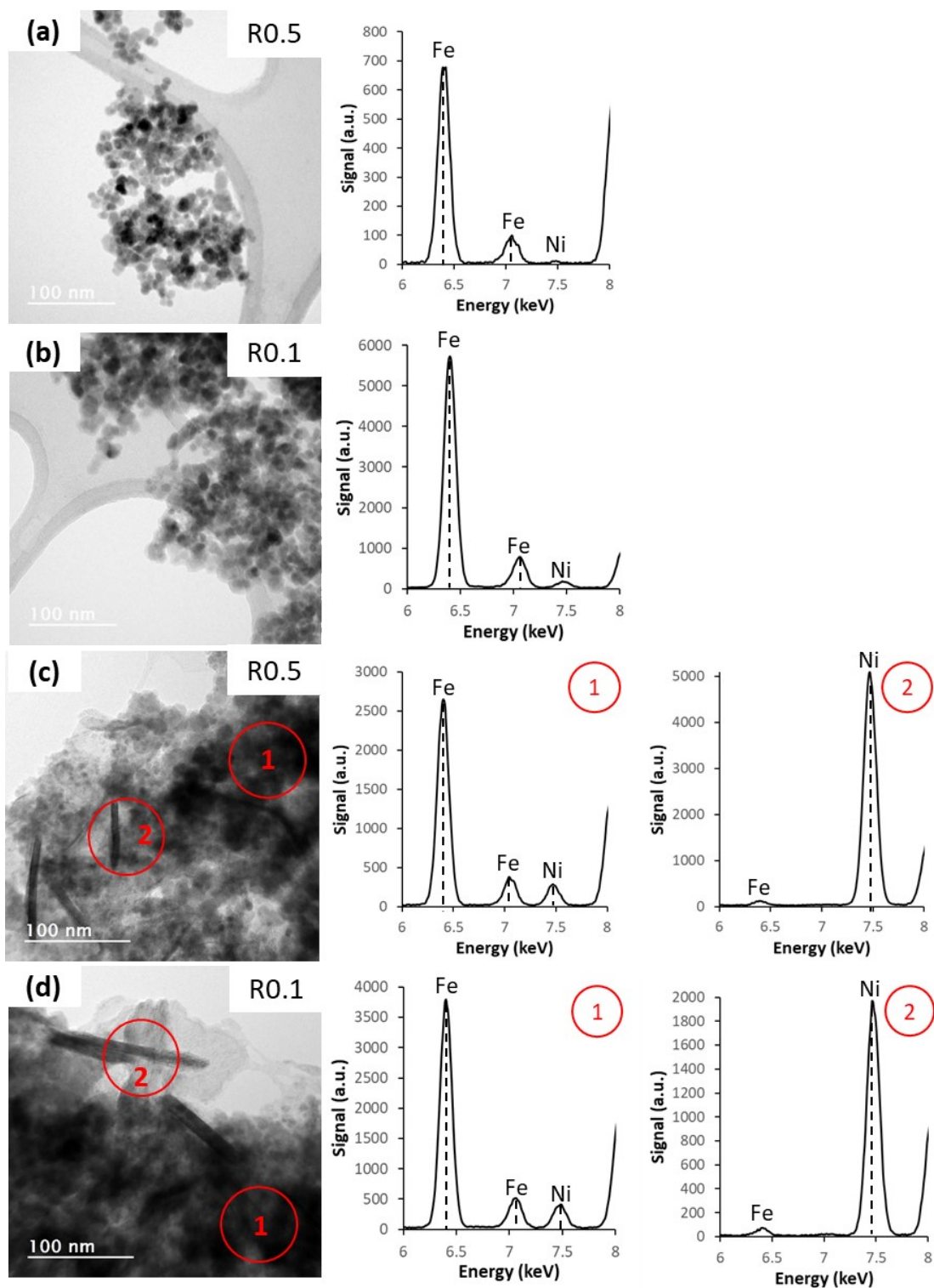


Fig. S1 TEM images with corresponding EDS (a) for R0.1 with $[\text{Ni}]_{\text{tot}} = 0.04$ mM ($[\text{Ni}]_{\text{s}} = 0.4$ atom nm^{-2}), (b) for R0.5 with $[\text{Ni}]_{\text{tot}} = 0.04$ mM ($[\text{Ni}]_{\text{s}} = 0.5$ atom nm^{-2}), (c) R0.1 with $[\text{Ni}]_{\text{tot}} = 3$ mM ($[\text{Ni}]_{\text{s}} = 22.6$ atom nm^{-2}) and (d) R0.5 with $[\text{Ni}]_{\text{tot}} = 3$ mM ($[\text{Ni}]_{\text{s}} = 20.5$ atom nm^{-2}). For the highest Ni concentrations, two spectra of EDS are available. The first one is the spectra of nanoparticles and the second one of nanosheets.

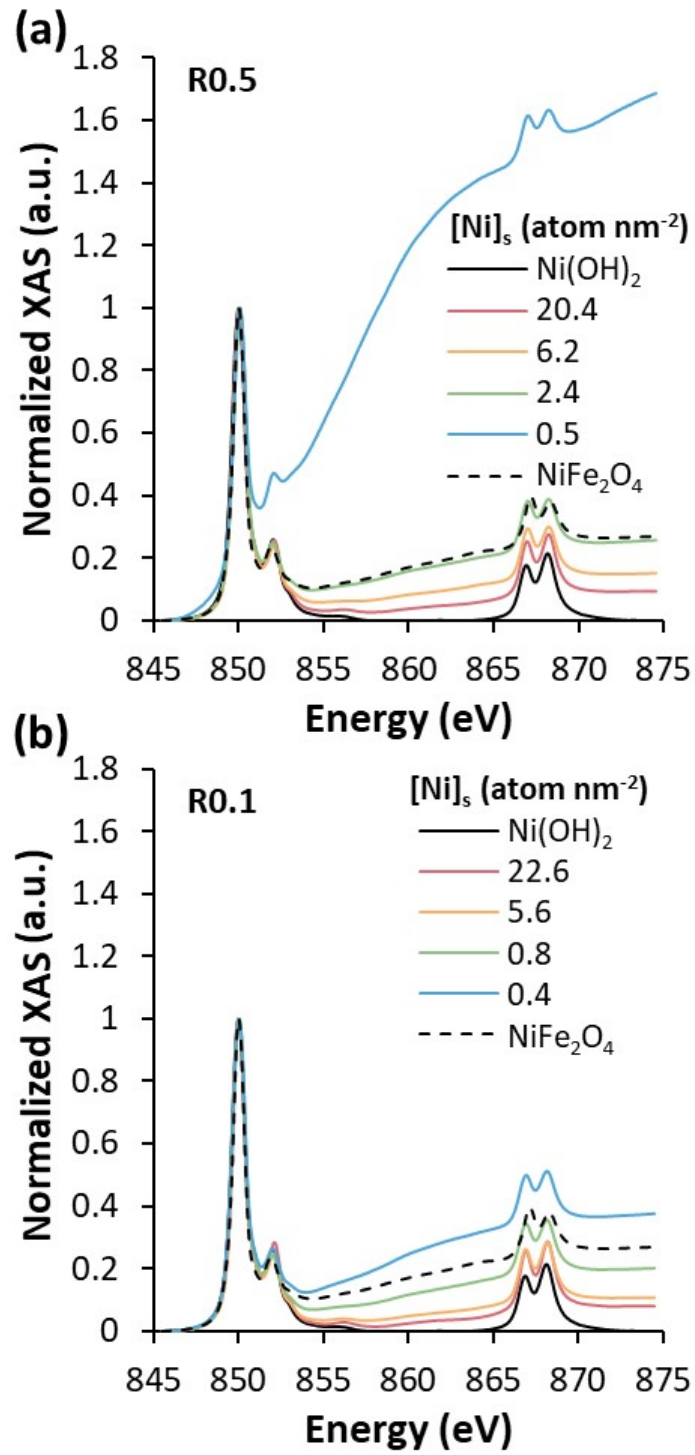


Fig. S2 Normalized XAS spectra at the Ni $L_{2,3}$ -edges, at 4.2 K and under 6.4 T, without background suppression for (a) R0.5 and (b) R0.1, for different Ni concentrations ($0.4 \leq [Ni]_s \leq 22.6$ atom nm^{-2}) and two references, $NiFe_2O_4$ and $Ni(OH)_2$. XAS signals are normalized by dividing the raw signal by the maximum XAS peak.

XMCD analysis. The normalized XMCD spectra are shown in Fig. S3 and are typical of Ni(II) in Oh sites with a main peak (noted E) at 850.2 eV.¹ The intensity of the most intense peak in the NiFe₂O₄ and Ni(OH)₂ references is -0.84 and -0.76 respectively. For R0.5, the signal intensity decreases from -1.04 to -0.78 with increasing Ni concentration. This is probably due to the presence of a ferrimagnetic phase NiFe₂O₄-like at low [Ni], followed by the formation of Ni(OH)₂-like phase. In the case of R0.1, the signal intensity varies between -0.72 and -0.62 depending on the [Ni]. The XMCD signal for [Ni]_s = 0.4 atom nm⁻² is lower than that of NiFe₂O₄ and equivalent to that of [Ni]_s = 22.6 atom nm⁻². The results suggest that interaction mechanisms between, Ni and R0.1 or R0.5 differ depending on [Ni]. The XAS and XMCD spectra at the Fe L_{2,3}-edges are presented in Fig. S4. The S ratio is 1.19 ± 0.05 for R0.5 and 0.89 ± 0.02 for R0.1, which is in agreement with the ratios found in the literature.²⁻⁶

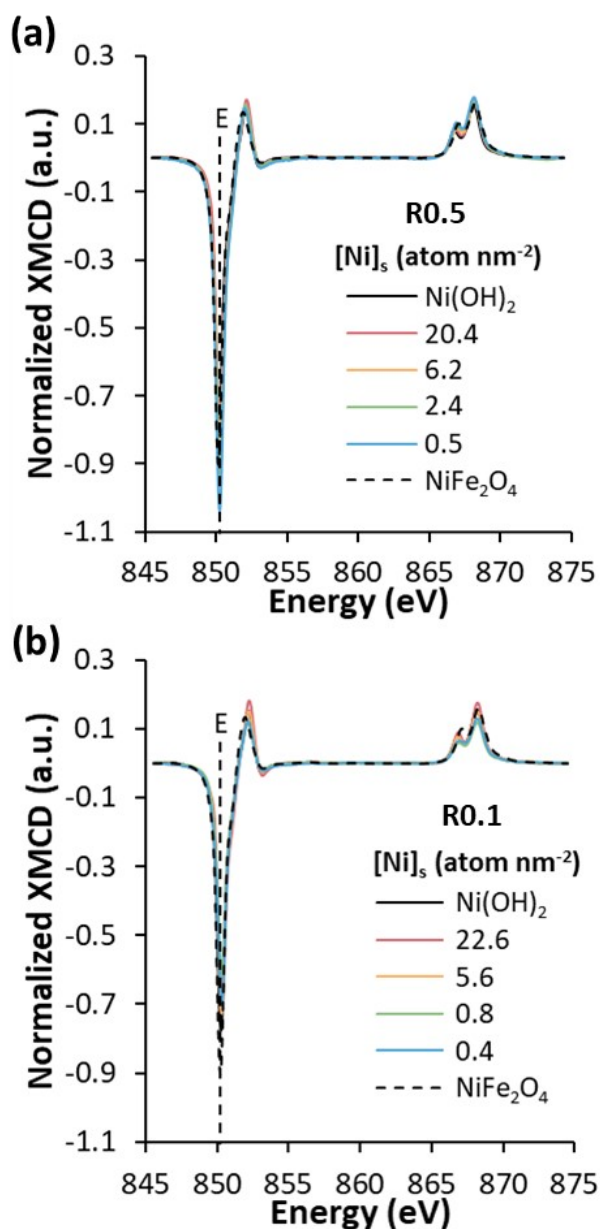


Fig. S3 Normalized XMCD spectra at the Ni L_{2,3}-edges, at 4.2 K and under 6.4 T, for (a) R0.5 and (b) R0.1 with different solid Ni concentrations ($0.4 \leq [\text{Ni}]_s \leq 22.6$ atom nm⁻²) and two references: NiFe₂O₄ (dotted line) and Ni(OH)₂ (full black line). XMCD signals are normalized by dividing the raw signal by the maximum XAS peak.

XMCD magnetization curves at Ni²⁺(Oh). In order to obtain additional information on the behavior of adsorbed and precipitated Ni on stoichiometric and non-stoichiometric magnetite, XMCD magnetization curves were recorded at a fixed energy, corresponding to the maximal intensity in the XMCD (at 850 eV). XMCD(H) curves (Fig. 4) showed different behaviors depending on the Ni surface loading and the stoichiometry. The Ni(OH)₂ magnetization curve presents an important unsaturation without a coercive field, which can be attributed to a paramagnetic behavior.⁷ At low Ni concentrations, [Ni]_s = 0.5 atom nm⁻² for R0.5 and 0.4 atom nm⁻² for R0.1, the magnetic behaviors are similar: saturation at high magnetic field with a coercive field. These behaviors are in great agreement with variation of XMCD signal versus the Ni concentration. These magnetization curves corresponded to a ferrimagnetic phase such as nickel ferrite.⁸ However, as Ni concentration increases, distinct behaviors are observed for R0.1 and R0.5. For R0.5, when [Ni]_s = 6.2 atom nm⁻², the magnetization curve still shows saturation, whereas for R0.1, when [Ni]_s = 5.6 atom nm⁻² saturation is not observed. At high Ni concentrations ([Ni]_s = 20.4 and 22.6 atom nm⁻² for R0.5 and R0.1 respectively) the magnetization curves present an unsaturation, which is close to the antiferromagnetic phase Ni(OH)₂ magnetization curve. Unsaturation is stronger for R0.1 than for R0.5, which corresponds to the larger proportion of NiFe₂O₄-like phase formed with R0.5 than with R0.1.

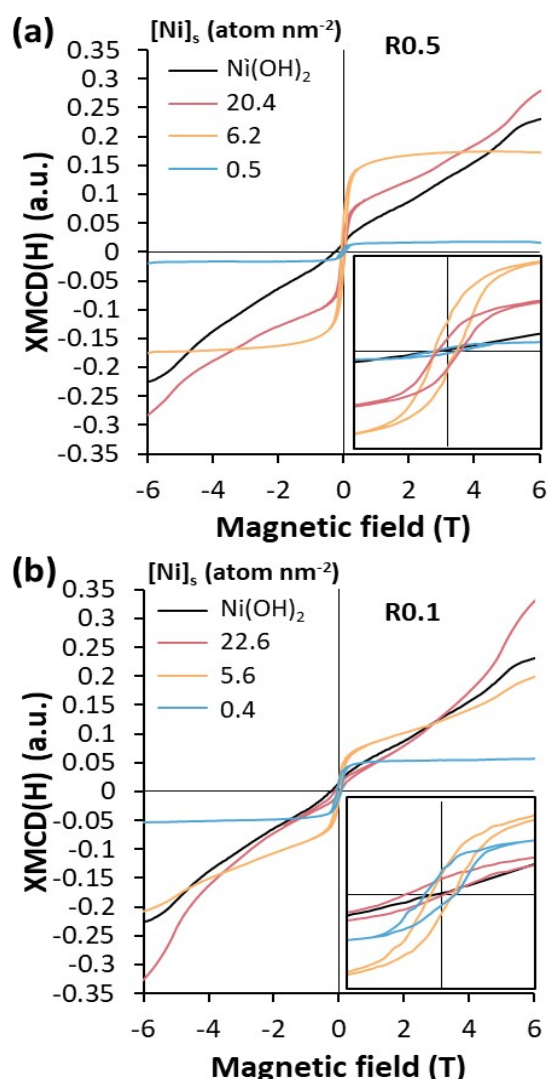


Fig. S4 XMCD magnetization versus magnetic fields measurement at the Ni L_3 -edge at 4.2 K for three solid Ni concentrations (from 0.4 to 22.6 atom nm⁻²) for (a) R0.5 and (b) R0.1.

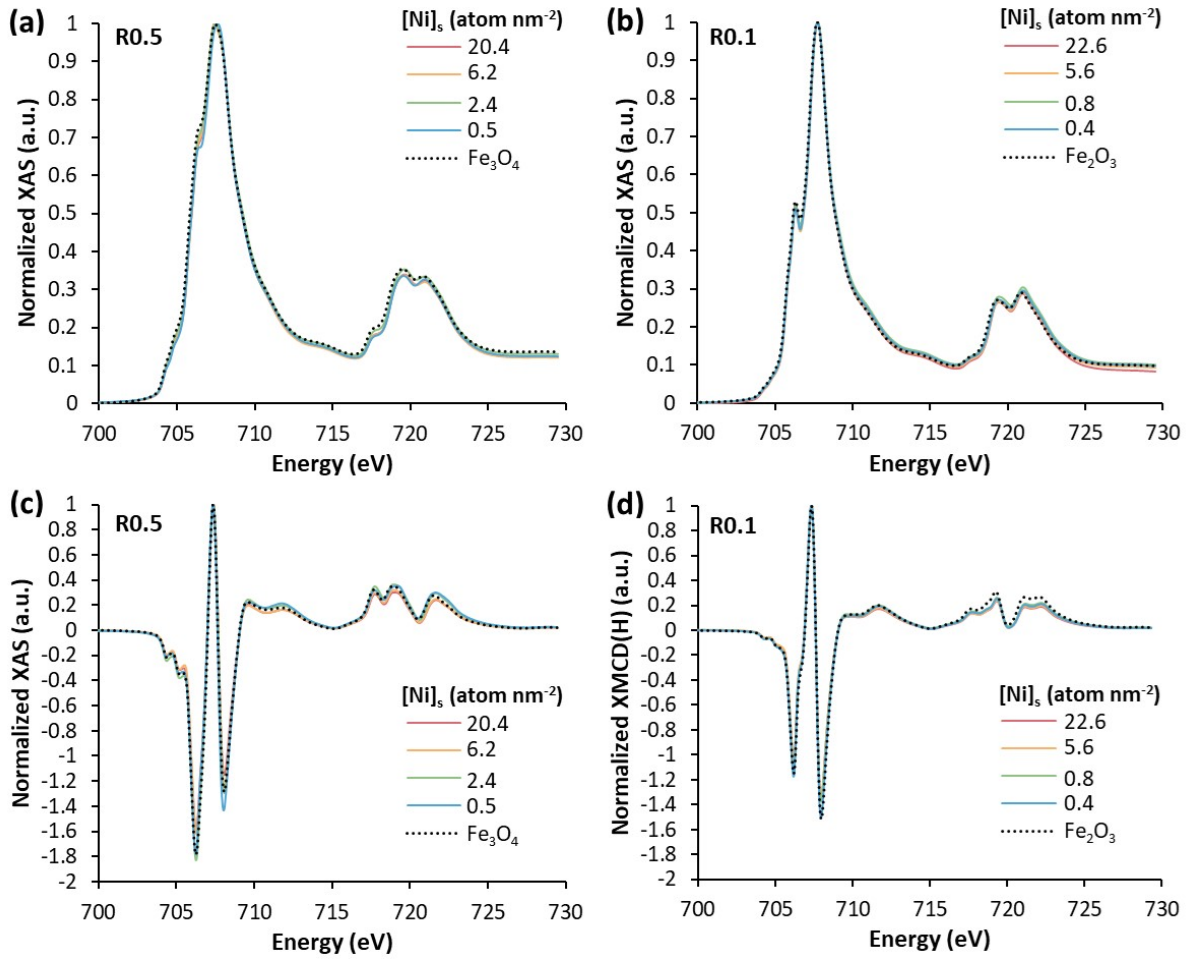


Fig. S5 Normalized XAS spectra for (a) R0.5 and (b) R0.1, and normalized XMCD spectra for (c) R0.5 and (d) R0.1, at the Fe $L_{2,3}$ -edges, at 4.2 K and under 6.4 T, with different solid Ni concentrations ($0.4 \leq [\text{Ni}]_s \leq 226 \text{ atom nm}^{-2}$) and two references : maghemite (Fe_2O_3) and magnetite (Fe_3O_4) represented by dotted line (data from Jungcharoen *et al.*, 2021).¹ XAS signals are normalized by dividing the raw signal by the edge jump of XAS. XMCD signals were normalized to the Fe(III)(Td) peak (positive one).

Table S2 Structural parameters deduced from the EXAFS analysis at the Ni *K*-edge for different Ni total concentrations (from 0.5 to 20.4 atom nm⁻²) on R0.5. CN: coordination number, R: interatomic distance (Å), σ^2 : Debye-Waller factor (Å²). E_0 is the energy shift parameter (eV). Uncertainties in CN, R and σ^2 are estimated to be $\pm 10\%$, 1% and 20% , respectively. For $[\text{Ni}]_{\text{tot}} = 0.04$ mM, the three Ni-Fe/Ni paths were fixed after preliminary adjustments. Fixed parameters are denoted by “*”.

Sample		Path				Parameters		
		Ni-O	Ni-Fe/Ni	Ni-Fe/Ni	Ni-Fe/Ni	E_0	Reduced-chi ²	R-factor
[Ni] _s = 0.5 atom nm ⁻²	CN	6.05	6.19*	6.19*	6.19*	-1.5	8.57	0.03
	R	2.05	2.98	3.52	5.14			
	σ^2	0.005	0.009	0.010	0.002			
[Ni] _s = 2.3 atom nm ⁻²	CN	5.9	5.5	4.5	5.5	-0.8	8.79	0.04
	R	2.06	3.01	3.52	5.14			
	σ^2	0.005	0.009	0.122	0.003			
[Ni] _s = 6.2 atom nm ⁻²	CN	6.0	4.07	3.6	4.5	-1.8	14.20	0.02
	R	2.05	3.02	3.53	5.14			
	σ^2	0.006	0.008	0.015	0.004			
[Ni] _s = 9.4 atom nm ⁻²	CN	6.0	4.5	3.3	3.9	-2.0	9.58	0.03
	R	2.05	3.04	3.55	5.15			
	σ^2	0.006	0.007	0.017	0.007			
[Ni] _s = 13.6 atom nm ⁻²	CN	5.9	4.1	2.4		-1.3	15.28	0.03
	R	2.05	3.07	3.61				
	σ^2	0.006	0.006	0.016				
[Ni] _s = 20.4 atom nm ⁻²	CN	6.0	3.8	1.8		-2.8	11.18	0.03
	R	2.04	3.07	3.54				
	σ^2	0.006	0.007	0.009				
Ni(OH) ₂	CN	5.5	5.8			-2.9	12.60	0.03
	R	2.04	3.09					
	σ^2	0.009	0.007					

Table S3 Structural parameters deduced from the EXAFS analysis at the Ni *K*-edge for different Ni total concentrations (from 0.4 to 22.6 atom nm⁻²) on R0.1. CN: coordination number, R: interatomic distance (Å), σ^2 : Debye-Waller factor (Å²). E_0 is the energy shift parameter (eV). Uncertainties in CN, R and σ^2 are estimated to be $\pm 10\%$, 1% and 20% , respectively. For $[\text{Ni}]_{\text{tot}} = 0.04$ mM, the three Ni-Fe/Ni paths were fixed after preliminary adjustments. Fixed parameters are denoted by “*”.

Sample		Path				Parameters		
		Ni-O	Ni-Fe/Ni	Ni-Fe/Ni	Ni-Fe/Ni	E_0	Reduced-chi ²	R-factor
[Ni] _s = 0.4 atom nm ⁻²	CN	5.9	3.5*	3.5*	3.5*	-2.3	10.50	0.06
	R	2.04	3.01	3.54	5.15			
	σ^2	0.005	0.008	0.010	0.004			
[Ni] _s = 0.8 atom nm ⁻²	CN	6.0	3.2	2.8	3.4	-2.0	7.32	0.03
	R	2.05	3.03	3.56	5.16			
	σ^2	0.006	0.006	0.012	0.006			
[Ni] _s = 5.6 atom nm ⁻²	CN	6.1	3.5	2.7		-3.0	6.81	0.02
	R	2.04	3.01	3.55				
	σ^2	0.006	0.008	0.015				
[Ni] _s = 10.2 atom nm ⁻²	CN	5.9	3.8	2.3		-2.2	2.80	0.02
	R	2.04	3.05	3.57				
	σ^2	0.006	0.007	0.014				
[Ni] _s = 12.5 atom nm ⁻²	CN	5.8	4.1	1.5		-1.0	21.09	0.03
	R	2.05	3.08	3.61				
	σ^2	0.007	0.006	0.008				
[Ni] _s = 22.6 atom nm ⁻²	CN	6.0	4.2	1.0		-2.7	11.61	0.02
	R	2.04	3.08	3.58				
	σ^2	0.005	0.006	0.007				
Ni(OH) ₂	CN	5.5	5.8			-2.9	12.60	0.03
	R	2.04	3.09					
	σ^2	0.009	0.007					

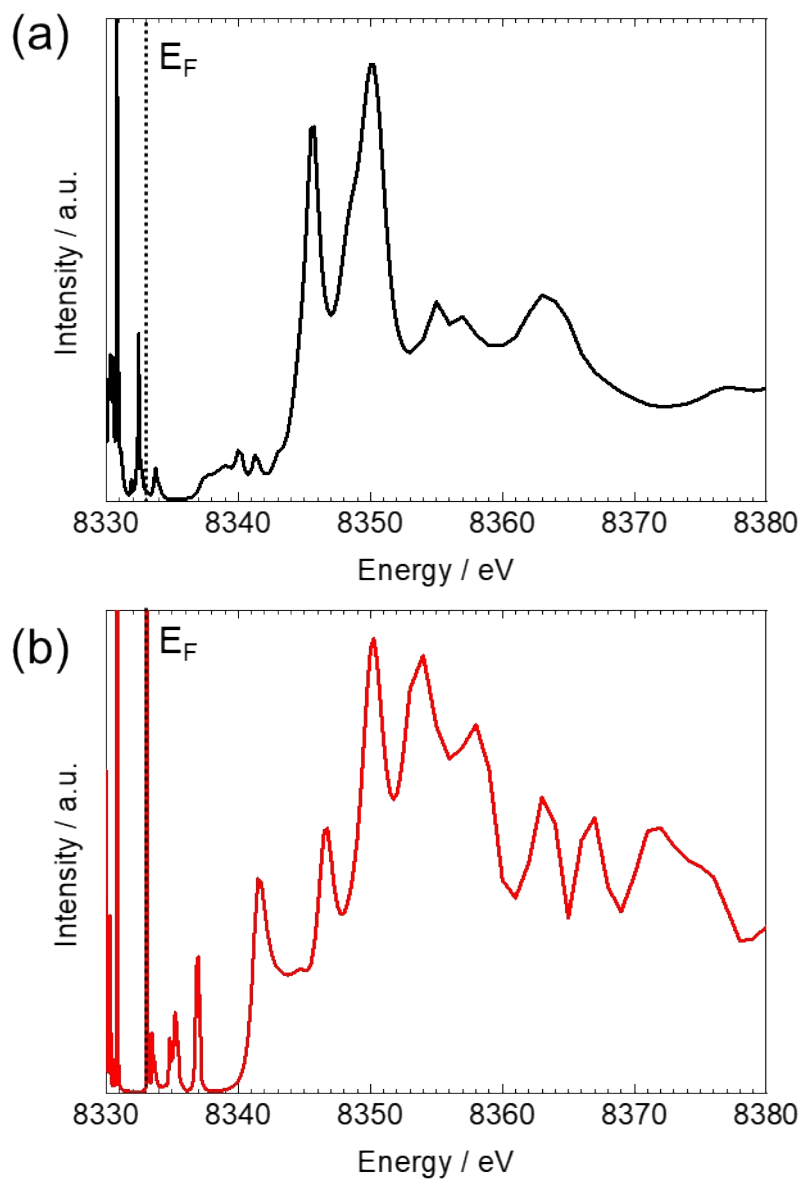


Fig. S6 Comparison of the theoretical Ni K edge XANES spectra of (a) $\text{Ni}(\text{OH})_2$ and (b) $\text{NiFe}_2\text{CrO}_4$. Fermi energy is shown by black dotted line.

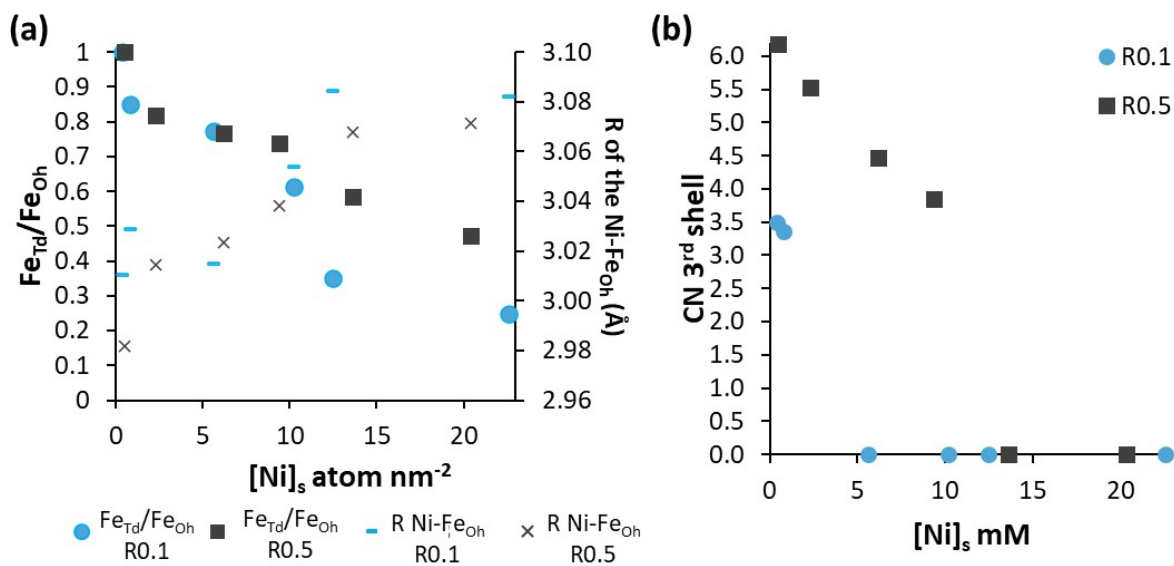


Fig. S7 (a) Ratio between the coordination number (CN) assigned to Fe_{Td} and the CN assigned to Fe_{Oh} relative to the concentration of solid Ni (in atom nm⁻²) for R0.1 (blue) and R0.5 (gray) magnetite, and on the second axis the interatomic distance (R) of the Ni-Fe_{Oh} path. (b) Determined coordination number (CN) of the third shell (Ni-Fe/Ni path at ~4.66 Å) for R0.1 (blue) and R0.5 (gray) magnetite.

References

- 1 V. S. Coker, C. I. Pearce, R. A. D. Patrick, G. van der Laan, N. D. Telling, J. M. Charnock, E. Arenholz and J. R. Lloyd, Probing the site occupancies of Co-, Ni-, and Mn-substituted biogenic magnetite using XAS and XMCD, *Am. Mineral.*, 2008, **93**, 1119–1132.
- 2 S. Larumbe, C. Gomez-Polo, J. I. Pérez-Landazábal, A. García-Prieto, J. Alonso, M. L. Fdez-Gubieda, D. Cordero and J. Gómez, Ni Doped Fe₃O₄ Magnetic Nanoparticles, *J. Nanosci. Nanotechnol.*, 2012, **12**, 2652–2660.
- 3 L. Fablet, F. Choueikani, M. Pédrot, M. Kerdiles, M. Pasturel and R. Marsac, Investigation of magnetite–Co interactions: from environmentally relevant trace Co levels to core–shell Fe₃O₄@Co(OH)₂ nanoparticles with magnetic applications, *Environ. Sci.: Nano*, 2023, **10**, 3051–3061.
- 4 P. Jungcharoen, M. Pédrot, F. Choueikani, M. Pasturel, K. Hanna, F. Heberling, M. Tesfa and R. Marsac, Probing the effects of redox conditions and dissolved Fe²⁺ on nanomagnetite stoichiometry by wet chemistry, XRD, XAS and XMCD, *Environ. Sci.: Nano*, 2021, **8**, 2098–2107.
- 5 P. Jungcharoen, M. Pédrot, F. Heberling, K. Hanna, F. Choueikani, C. Catrouillet, A. Dia and R. Marsac, Prediction of nanomagnetite stoichiometry (Fe(II)/Fe(III)) under contrasting pH and redox conditions, *Environ. Sci.: Nano*, 2022, **9**, 2363–2371.
- 6 E. Pellegrain, M. Hagelstein, S. Doyle, H. O. Moser, J. Fuchs, D. Vollath, S. Schuppler, M. A. James, S. S. Saxena, L. Niesen, O. Rogojanu, G. A. Sawatzky, C. Ferrero, M. Borowski, O. Tjernberg and N. B. Brookes, Characterization of Nanocrystalline γ -Fe₂O₃ with Synchrotron Radiation Techniques, *Phys. Status Solidi (B): Basic Res.*, 1999, **215**, 797–801.
- 7 S. R. Yousefi, D. Ghanbari, M. Salavati-Niasari and M. Hassanpour, Photo-degradation of organic dyes: simple chemical synthesis of Ni(OH)₂ nanoparticles, Ni/Ni(OH)₂ and Ni/NiO magnetic nanocomposites, *J. Mater. Sci.: Mater. Elect.*, DOI:10.1007/s10854-015-3882-6.
- 8 S. Karmakar and D. Behera, Magnetic and Optical Studies of NiFe₂O₄ Micro- and Nanoparticles, *J. Supercond. Nov. Magn.*, 2020, **33**, 1619–1627.